2020 IEEE 21st International Workshop on Signal Processing Advances in Wireless Communications (SPAWC)

Multi-Array Designs for mmWave and Sub-THz Communication to UAVs

William Xia[†] Vasilii Semkin[♭] Marco Mezzavilla[†] Giuseppe Loianno[†] Sundeep Rangan[†]
[†]NYU Tandon School of Engineering, Brooklyn, NY, USA
[♭]VTT Technical Research Centre of Finland Ltd, Finland

***Abstract*—Unmanned Aerial Vehicles (UAVs) are steadily being considered for scenarios demanding high bandwidth, low latency communications for video and sensor data transfer as well as real-time control. UAVs may also be used as mobile aerial Base Station (BS) for maintaining the communication in emergency scenarios. The millimeter wave (mmWave) bands, including the sub-THz frequencies above 100 GHz, are an attractive technology for high data rate UAV connectivity due to the wide bandwidths available at these frequencies. This paper studies antenna and codebook design for UAV communication at both 28 and 140 GHz with realistic antenna simulations and flight patterns. The analysis shows that multi-array configurations with proper codebook design are necessary for uniform spherical coverage and become particularly important in long range applications. The paper thus proposes a four array design with patch antennas. Simulations indicate that the design can achieve in excess of 1 Gbps data rates at a range of 1 km, with reasonable power levels and moderate rain fades. A simulation with a real public safety mission flight shows that beam tracking can be maintained even under high drone movements and rotations.**

***Index Terms*—UAV, mmWave, sub-THz, beamforming, codebook design, antenna placement**

I. INTRODUCTION

High-data rate connectivity is becoming increasingly important in UAVs to support real-time sensor and camera data transfer, remote control, and situations when the UAV acts as an aerial base station. For these applications, the millimeter wave (mmWave) bands offer large bandwidths that can support massive data rates at low latency [1], [2]. In addition, links to UAVs are often line-of-sight (LOS) and thus avoid blockage problems common in mmWave cellular and LAN deployments [3], [4]. Nevertheless, mmWave UAV communication present several technical challenges including range, power consumption and directional tracking in high mobility scenarios. The goal of this work is to evaluate the performance of UAV mmWave communications with realistic implementations of codebook-based beamforming, beam search techniques, and antenna radiation patterns.

Prior work in mmWave UAV communication is relatively recent. For example, [4] performed laboratory experiments and evaluated the beam tracking performance. Similarly, [3] performed ray tracing and channel sounding to evaluate 28 and 60 GHz UAV-ground channels. The work [5] developed a codebook design procedure for beam coverage for a given target area. Multi-user MIMO communication with several aircrafts connected to a central hub was studied in [6]. Several applications have also been simulated: for example, [7] evaluated UAV-ground communication in a public safety scenario and [8] studied the possibility of mmWave UAV backhaul.

This paper considers multi-array designs and more detailed antenna modeling. We demonstrate that the antenna design and placement can greatly affect the communication range and multi-array designs can offer significant benefits in long-range applications. In contrast to most prior work, we also consider communication above 100 GHz where the bandwidths are even larger than the lower mmWave frequencies. Specifically, we study two systems: (a) a 28 GHz system similar to the configuration for a 5G New Radio (NR) [9] mmWave deployment today; and (b) a hypothetical 140 GHz system, also using an NR-type link. The 140 GHz band is the most likely sub-THz frequency for future 6G systems [10].

II. ANTENNA AND BEAMFORMING MODEL

We use the 3GPP New Radio (NR) terminology [9] where the UAV is the user equipment (UE) and the ground base station is the gNB. We focus on the uplink (UE → gNB) since it is the most power constrained. We suppose the UAV has $N_{\rm arr}$ antenna arrays, each array with $N_{\rm UE}$ antenna elements. We index the arrays by $k = 1, \ldots, N_{\rm arr}$ and assume all elements in the same array have the same orientation. Thus, in each array k, the elements have an identical *element gain*, $A_E^{(k)}(\theta, \phi)$, representing the power gain of a plane wave arriving with elevation and azimuth angles θ and ϕ onto an element in array k. In addition each array is characterized by a *spatial signature*, $\mathbf{u}_k(\theta, \phi) \in \mathbb{C}^{N_{\rm UE}}$ which represents the complex response of the $N_{\rm UE}$ antennas to a plane wave with angles θ and ϕ. We will assume the components of the spatial signature are normalized as $|u_{k\ell}|= 1$. Thus, each direction results in a vector of phase shifts defining its spatial signature.

We assume the UAV transmits from only one array at a time. Thus, at each time, the UE will select an array k and apply a *beamforming vector* $\mathbf{w} \in \mathbb{C}^{N_{\rm UE}}$. We assume $\|\mathbf{w}\|= 1$. The resulting *total transmit gain* in a direction (θ, ϕ) is then,

$$G(\theta, \phi, \mathbf{w}) = A_E^{(k)}(\theta, \phi) + A_{\rm BF}^{(k)}(\theta, \phi, \mathbf{w}), \tag{1}$$

where $A_{\rm BF}^{(k)}(\cdot)$ is the beamforming gain,

$$A_{\rm BF}^{(k)}(\theta, \phi, \mathbf{w}) := 10 \log_{10} |\mathbf{u}_k(\theta, \phi) \cdot \mathbf{w}|^2, \tag{2}$$

where $\mathbf{a} \cdot \mathbf{b}$ denotes the dot product between vectors $\mathbf{a}$ and $\mathbf{b}$.

978-1-7281-5478-7/20/$31.00 ©2020 IEEE

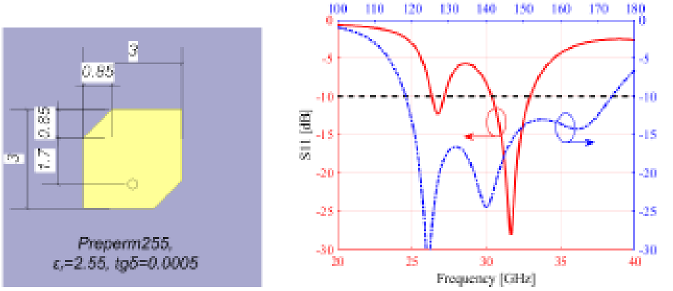

(a) Geometry of circular polarized patch antenna element operating at 28 GHz.

(b) Reflection coefficient for patch antennas optimized at 28 (red line) and 140 GHz (blue line).

Fig. 1: Proposed antenna structure.

We will assume a line-of-sight (LOS) channel with a single direction of arrival (θ, ϕ). In this case, the maximum of the total transmit gain in (1) is,

$$G^{\max}(\theta,\phi) = \max_{k} \max_{\mathbf{w}} \left[A_E^{(k)}(\theta,\phi) + A_{\text{BF}}^{(k)}(\theta,\phi,\mathbf{w}) \right], \quad (3)$$

where the maximization is over the array selection k and the beamforming vector $\mathbf{w}$. We will use the value of the maximum (3) to evaluate various design parameters including the antenna element design, array layout, placement and beamforming codebook.

III. ANTENNA DESIGN

Antenna Element design: For the 28 GHz case, we consider a single circular polarized patch antenna element on a low loss Preperm255 substrate ($\epsilon_r = 2.55$, and tanδ = 0.0005) with thickness of 0.5 mm. Patch antenna element has two opposite corners truncated to provide circular polarization (CP) [11] and the feeding point of the patch is offset from the center by 1.05 mm for antenna optimized at 28 GHz (Fig. 1a). Similar antenna geometry is considered at 140 GHz, antenna is designed on a 3 layer Megtron7 substrate with $\epsilon_r = 3.4$ and tanδ = 0.002. The CP antennas may be beneficial for communications since the position of the drone can be arbitrary during the flight. The following parameters are obtained during the electromagnetic simulations in Ansys HFSS: axial ratio is 5.5 dB; maximum gain is 7.2 dBi; and the half power beam width (HPBW) is 82° for single antenna element operating at 28 GHz. The axial ratio is 1.25 dB and the gain is 5.2 dBi for the antenna operating at 140 GHz. The reflection coefficient of the developed antenna elements is presented in Fig. 1b. Further optimization of the antenna element can be performed (e.g. by adding a partially reflecting surface [12]) to achieve larger bandwidth and higher gain of the array, however, this is out of the scope of this work but will be considered in the future.

Array configuration and placement: We consider two realistic array configurations:

- A **single array** located on the bottom of the drone to provide coverage of the bottom hemisphere (Fig. 2a);
- **Four antenna arrays** located on the sides of the drone and tilted by $-45°$ relative to the drone plane (Fig. 2b). Each array covers an approximately 90° sector.

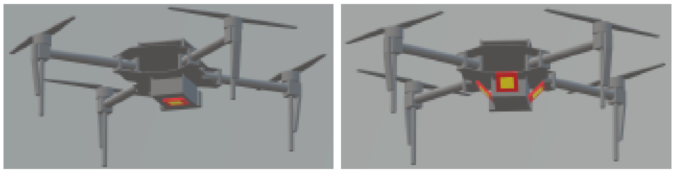

(a) Single antenna array under the drone.

(b) Four antenna arrays on the sides of the drone.

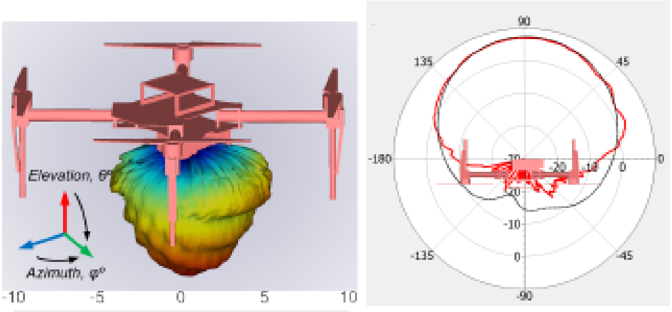

(c) Radiation pattern of a single patch antenna element mounted on the bottom of the drone.

(d) Radiation pattern for single element at $\theta \in [-180, 180]°$, $\phi = 0°$. Black line-initial pattern, red line-antenna on the drone.

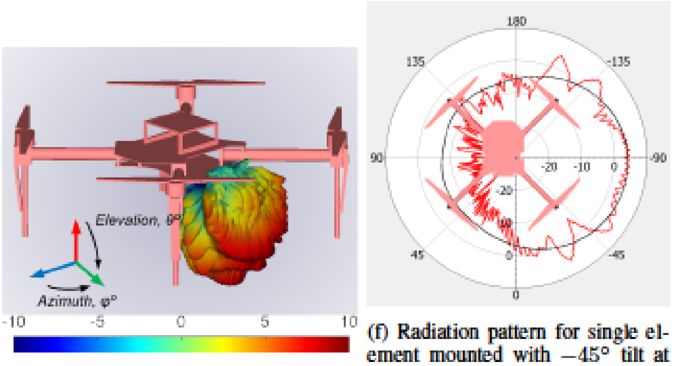

(e) Radiation pattern of single patch antenna element tilted to $-45°$ mounted on one side of the drone.

(f) Radiation pattern for single element mounted with $-45°$ tilt at $\theta = 135°$, $\phi \in [-180, 180]°$. Black line-initial pattern, red line-antenna on the drone.

Fig. 2: Antenna configurations and estimated radiation patterns on a commercial drone at 28 GHz.

In order to estimate the effect of the drone frame on the antenna parameters, we performed shooting and bouncing ray (SBR) simulations using geometrical optics (GO) using a real 3D model for a commercial drone. This is a typical quadcopter with the diagonal dimension of 650 mm. Usually, large drones are made of carbon fiber, while in the simulations we use PEC material to simplify the model and and similar characteristics. At the current time, our SBR simulations are only performed at 28 GHz. We assume that we can obtain similar radiation patterns at 140 GHz, however the effect of the drone frame might be severe at higher frequencies. Our future work includes studies mentioned above. Figs. 2c and 2e shows the estimated 3D radiation patterns, as well as, azimuth and elevation cuts of the single antenna element located in the single and four array cases. For the four array case, the patterns from only one of the four arrays are shown – the others are identical by symmetry. Figs. 2d and 2f also compare the radiation patterns (dash black line - antenna in the free space and solid red line - antenna on the drone). We see that drone body affects on the radiation patterns may be significant.

IV. MULTI-ARRAY CODEBOOK DESIGN

In many cases, search can only be performed over a discrete set of beamforming vectors or *codebook*. Good codebook design is necessary to obtain good beamforming in all directions of interest. To this end, we extend the Lloyd-type codebook design algorithm in [13] for multi-arrays. Let $\mathcal{S}^{(k)} = \{\boldsymbol{w}_1^{(k)}, \ldots, \boldsymbol{w}_M^{(k)}\}$ be the codebook for array k, where M is the number of beamforming vectors in the codebook. Typically, we set $M = N_{\rm UE}$ so that the number of codebook vectors equals the number of spatial degrees of freedom. The goal is to select the set of codebooks, $\mathcal{S} = (\mathcal{S}^{(1)}, \ldots, \mathcal{S}^{(N_{\rm arr})})$.

To this end, we select a large number of random angles (θ_i, ϕ_i), $i = 1, \ldots, N$, from the distribution over which we desire coverage. In this study, we draw the vectors uniformly over the bottom hemisphere of the UAV, specifically $\theta \in [-90, 0]$ and $\phi \in [-180, 180]$. We use this distribution since in many applications (one of which is simulated in Sec. V-D), the drone receives communication signals from a negative elevation angle for most of its flight.

Then, given a set of codebooks, $\mathcal{S}$, the expected maximum beamforming gain is,

$$J(\mathcal{S}) := \frac{1}{N} \sum_{i=1}^{N} \max_k \max_j |\boldsymbol{w}_j^{(k)} \cdot \boldsymbol{u}_k(\theta_i, \phi_i)|^2, \qquad (4)$$

where $\boldsymbol{u}_k(\theta_i, \phi_i)$ is the spatial signature for the i-th direction on array k. The expected beamforming gain is then maximized iteratively:

- Given a set of codebooks, $\mathcal{S}$, for each direction i, we select the array $\hat{k}_i$ and codebook vector index $\hat{j}_i$ that achieves the maximum beamforming gain in (4);
- For each k and j, let I_{kj} be the set of directions i such that $\hat{k}_i = k$ and $\hat{j}_i = j$.
- Update the codebook vector $\boldsymbol{w}_j^{(k)}$ to maximize,

$$\boldsymbol{w}_j^{(k)} = \arg\max_{\boldsymbol{w}} \sum_{i \in I_{jk}} |\boldsymbol{w} \cdot \boldsymbol{u}_k(\theta_i, \phi_i)|^2. \qquad (5)$$

This maximum in (5) is given by the maximum eigenvector of

$$\sum_{i \in I_{jk}} \boldsymbol{u}_k(\theta_i, \phi_i) \boldsymbol{u}_k(\theta_i, \phi_i)^{\mathsf{H}}. \qquad (6)$$

The above three steps are repeated until convergence.

V. SIMULATION RESULTS

A. Parameters

We evaluate the antenna and codebook design for the parameters in Table I. As described in the Introduction, we consider both a 5G-like 28 GHz system and a hypothetical 140 GHz system for possible 6G applications. Note that the 140 GHz system requires significantly more power to support the wider bandwidths and would be intended for larger drones. For both systems, we assume an NR-like channel allocation where the bandwidth would be typically divided into component carriers using carrier aggregation [21], [22]. Similar parameters are used in [23]. We assume state-of-the-art reported mmWave device parameters for both the power amplifier (PA) [14], [15] and low noise amplifier (LNA) [18]–[20]. The path loss includes atmospheric loss at moderate rain levels (4mm/hr) [17].

TABLE I: System parameters

Parameter	**Value**		**Remarks**
Carrier frequency f_c	28 GHz	140 GHz	
Occupied bandwidth, B (GHz)	0.400	1.6	Typ. for 100 or 200 MHz component carriers.
UAV TX total power, $P_{\rm UE}$ (dBm)	23	26	
PA efficiency (%)	20	9.7	Values from [14], [15] with backoff
UAV PA power (W)	1.0	4.1	
Number UAV / UE antennas, $N_{\rm UE}$	16	64	4×4 and 8×8 UPAs
Number ground / gNB antennas, $N_{\rm gNB}$	64	256	
Rain Fade (dB/km)	0.7	5	Values from [16], [17] at 4mm/hr
Noise Figure (dB)	3.1	5.2	From [18]–[20]
Rate model	Eqn. (8)		

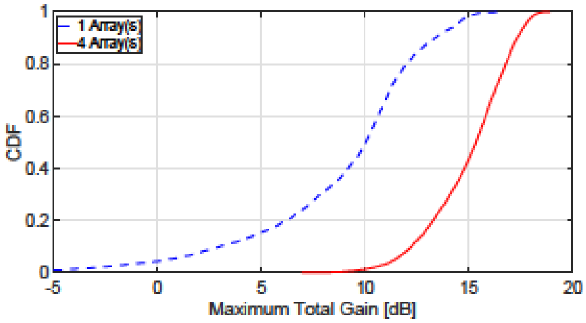

Fig. 3: Cumulative Distribution Function (CDF) of the coverage for multi-array configurations

B. Directional Coverage

Using the antenna patterns in Section III and the multi-array beamforming codebook design procedure in Section IV, Fig. 4 shows the total directional gain $G^{\max}(\theta, \phi)$ in (3) for angles (θ, ϕ) uniformly over the lower hemisphere. The figure plots the gains for 28 GHz carrier for one and four arrays with 4×4 elements per array. As expected, the single array configuration has poor coverage along the horizontal of the array at θ close to 0° in Fig. 4a. As we will see below, at long distances from the base stations, the signal often arrives close to horizontal and the low gain at these angle can significantly reduce the range. The multi-array configuration in contrast offers much more uniform lower hemisphere coverage. For example, the CDF in Fig. 3 clearly shows that the single array configuration has about 20% of the hemisphere having maximum total gain less than 5 dB. In contrast, nearly all of the directions for the four-array configuration achieve a maximum gain of over 10 dB with a median gain of about 15 dB.

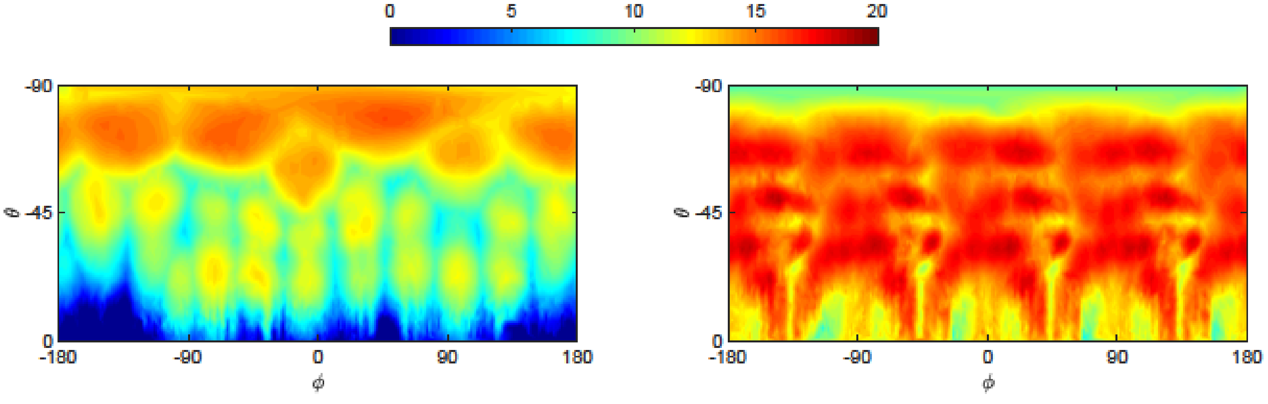

(a) Single 4×4 array (b) Four 4×4 arrays

Fig. 4: Total directional gains at 28 GHz

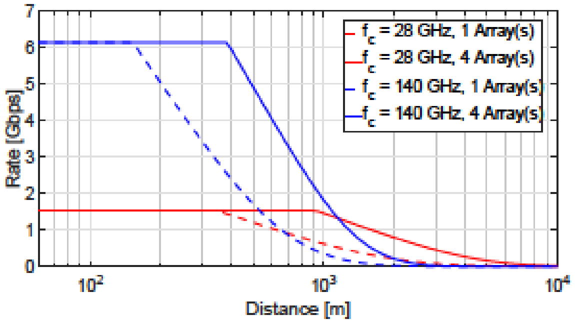

Fig. 5: Rate vs. distance for 28 and 140 GHz systems

C. Link Budget

To assess the link budget, Fig. 5 shows the expected data rate as a function of distance for the 28 and 140 GHz systems using the parameters in Table I. In each case, we assume the UAV is at an altitude of 35m above the ground base station. We assume the SNR is given by,

$$\mathrm{SNR} = 10\log_{10}\left(\frac{P_{\mathrm{UE}}G_{\mathrm{UE}}G_{\mathrm{gNB}}}{LB(kT)(NF)}\right), \tag{7}$$

where P_{UE} is the UE transmit power; G_{UE} and G_{gNB} are the total directional gain (element gain + beamforming gain) at the UE and gNB; L is the free space path loss, B is the bandwidth; kT is the thermal noise spectral density (for $T = 293\ K$) and NF is the noise figure. For the UE at 28 GHz, the gain $G_{\mathrm{UE}} = G^{\max}(\theta,\phi)$ is the gain with optimally selected array and codebook vector as computed in Section V-B. We assumed the gain for 140 GHz would scale with the number of antennas. For the gNB, we assume we can obtain a total gain (in dBi) given by $G_{\mathrm{gNB}} = 10\log_{10}(N_{\mathrm{gNB}}) + A_E$ where N_{gNB} is the number of antennas at the gNB and A_E is the gNB element gain which we take as $A_E = 5$ dBi. Given the SNR, the rate is then computed by the LTE-like model [24],

$$R = (1-\alpha)B\min\{\rho_{\max}, \log(1+10^{0.1(\mathrm{SNR}-\Delta)}\}, \tag{8}$$

where $\alpha = 0.2$ is the bandwidth loss (due to control signaling), $\Delta = 6$ dB is the SNR loss (due to receiver implementations) and $\rho_{\max} = 4.8$ bps/Hz is the maximum spectral efficiency.

Under these assumptions, we see that the four-array configuration offers significantly greater range than the single array configuration due to its ability to obtain high directivity at horizontal angles. We also see that the 140 GHz configuration can obtain peak rates in excess of 6 Gbps, and both the 28 and 140 GHz systems can achieve over 1 Gbps at a distance of 1 km.

D. Mission Flight Example

We conclude with an evaluation in a real drone trace using data that was provided by the Austin Fire Department (AFD) for a public safety communication scenario. This drone flight was first studied in [7]. In this simulation, the ground base station (gNB) is located at $(-700, 0, 25)$ m and the UAV has a flight path shown in Fig. 6. It is important to clarify that the base station is positioned at $x = -700$ and is thus about 700 m away from the starting position of the UAV flight path.

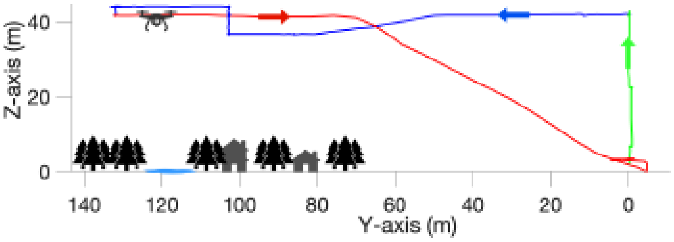

Fig. 6: Public Safety Mission Flight

Using the identical assumptions as in the link budget calculations, Fig. 7 plots the Signal to Noise Ratio (SNR) for a UAV taking the flight path shown by Fig. 6. The SNR is computed for carrier frequencies of both 28 GHz and 140 GHz and the SNR trace is color-matched to the different parts of the flight path for reference. Since the UAV is flying mostly perpendicular to the vector from the UAV to the gNB , the total distance does not change significantly over the flight. Hence the average SNR is roughly constant. However, the small SNR variation is due to rotational motion of the drone. We also have modeled the beamforming tracking error. Specifically, we

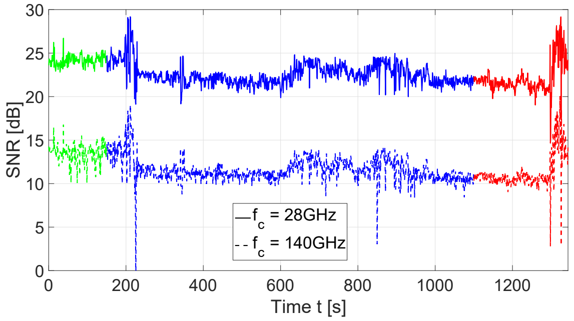

Fig. 7: Signal-to-Noise Ratio for public safety mission "Crowd Overwatch" from [7]

assume there is a 20 ms delay in beam search consistent with Primary Synchronization Signal (PSS) beam search in the NR standard [25]. We see that the SNR fluctuations are somewhat higher in the 140 GHz case due to the narrower beams.

VI. CONCLUSIONS

To assess the feasibility of mmWave communication to UAVs, we have conducted detailed simulations of a circularly polarized patch antenna element to evaluate the radiation pattern while also considering the effect of a real drone frame on the coverage. Using this antenna design, we propose and simulate two possible configurations for antenna array placement on a UAV and provide results for hemispheric coverage and gain distribution, link budget, and finally SNR for a real Public Safety Communication (PSC) flight for both mmWave and sub-THz bands. Our results show significant benefits for multi-array systems, particularly at long ranges. Indeed, with four arrays, we can maintain high gain throughout the lower hemisphere and obtain over 1 Gbps even at a 1 km distance and moderate rain fades. Using the proposed multi-array design, the maximum distance for which the system maintains the highest achievable throughput is in fact extended by over 600 m and 200 m for mmWave and sub-THz models, respectively. Future work will include more detailed modeling of the 140 GHz antennas as well as blockage analysis for low altitude flights.

Acknowledgements: W. Xia, M. Mezzavilla and S. Rangan were supported in part by NSF grants 1302336, 1564142, 1547332, and 1824434, NIST, SRC, and the industrial affiliates of NYU WIRELESS. The authors would like to thank Jaakko Haarla and Matti Somersalo for help with the simulations.

REFERENCES

[1] C. Zhang, W. Zhang, W. Wang, L. Yang, and W. Zhang, "Research Challenges and Opportunities of UAV Millimeter-Wave Communications," *IEEE Wireless Communications*, vol. 26, no. 1, pp. 58–62, 2019.

[2] M. Mozaffari, W. Saad, M. Bennis, and M. Debbah, "Communications and Control for Wireless Drone-Based Antenna Array," *IEEE Transactions on Communications*, vol. 67, no. 1, pp. 820–834, 2019.

[3] W. Khawaja, O. Ozdemir, and I. Guvenc, "UAV Air-to-Ground Channel Characterization for mmWave Systems," in *Proc. IEEE VTC-Fall*, 2017.

[4] K. Heimann, J. Tiemann, S. Boecker, and C. Wietfeld, "On the Potential of 5G mmWave Pencil Beam Antennas for UAV Communications: An Experimental Evaluation," in *WSA 2018; 22nd International ITG Workshop on Smart Antennas*, 2018, pp. 1–6.

[5] L. Zhu, J. Zhang, Z. Xiao, X. Cao, D. O. Wu, and X. Xia, "3-D Beamforming for Flexible Coverage in Millimeter-Wave UAV Communications," *IEEE Wireless Communications Letters*, vol. 8, no. 3, pp. 837–840, 2019.

[6] T. Cuvelier and R. W. Heath, "MmWave MU-MIMO for Aerial Networks," in *15th International Symposium on Wireless Communication Systems (ISWCS)*, 2018, pp. 1–6.

[7] W. Xia, M. Polese, M. Mezzavilla, G. Loianno, S. Rangan, and M. Zorzi, "Millimeter Wave Remote UAV Control and Communications for Public Safety Scenarios," in *16th Annual IEEE International Conference on Sensing, Communication, and Networking (SECON)*, 2019.

[8] M. Gapeyenko, V. Petrov, D. Moltchanov, S. Andreev, N. Himayat, and Y. Koucheryavy, "Flexible and Reliable UAV-Assisted Backhaul Operation in 5G mmWave Cellular Networks," *IEEE Journal on Selected Areas in Communications*, vol. 36, no. 11, pp. 2486–2496, 2018.

[9] 3GPP, "TS 38.300, NR and NG-RAN Overall Description; Stage 2," 2017.

[10] Y. Xing and T. S. Rappaport, "Propagation Measurement System and Approach at 140 GHz-Moving to 6G and Above 100 GHz," in *Proc. IEEE GLOBECOM*, 2018, pp. 1–6.

[11] C. A. Balanis, *Antenna Theory: Analysis and Design*. Wiley-Interscience, 2005.

[12] N. Hussain, M. Jeong, J. Park, and N. Kim, "A Broadband Circularly Polarized Fabry-Perot Resonant Antenna Using A Single-Layered PRS for 5G MIMO Applications," *IEEE Access*, vol. 7, pp. 42 897–42 907, 2019.

[13] P. Xia and G. B. Giannakis, "Design and Analysis of Transmit-Beamforming Based on Limited-Rate Feedback," *IEEE Transactions on Signal Processing*, vol. 54, no. 5, pp. 1853–1863, 2006.

[14] B. Sadhu *et al.*, "A 28-GHz 32-Element TRX Phased-Array IC with Concurrent Dual-Polarized Operation and Orthogonal Phase and Gain Control for 5G Communications," *IEEE Journal of Solid-State Circuits*, vol. 52, no. 12, pp. 3373–3391, 2017.

[15] S. H. Ahmed, A. A. Farid, M. Urteaga, J. Buckwalter, and M. J. W. Rodwell, "A 140GHz Power Amplifier with 20.5dBm Output Power and 20.8% PAE in 250-nm InP HBT Technology," in *Submitted to IEEE International Microwave Symposium (IMS)*, 2020.

[16] M. J. Rosker and H. B. Wallace, "Imaging Through the Atmosphere at Terahertz Frequencies," in *Proc. IEEE/MTT-S International Microwave Symposium*, 2007, pp. 773–776.

[17] H. J. Liebe, T. Manabe, and G. A. Hufford, "Millimeter-Wave Attenuation and Delay Rates Due to Fog/Cloud Conditions," *IEEE Transactions on Antennas and Propagation*, vol. 37, no. 12, pp. 1612–1617, 1989.

[18] Z. Chen, H. Gao, D. Leenaerts, D. Milosevic, and P. Baltus, "A 29–37 GHz BiCMOS Low-Noise Amplifier with 28.5 dB Peak Gain and 3.1-4.1 dB NF," in *Proc. IEEE RFIC*, 2018, pp. 288–291.

[19] A. Simsek, S.-K. Kim, and M. J. Rodwell, "A 140 GHz MIMO Transceiver in 45 nm SOI CMOS," in *Proc. IEEE BICMOS and Compound Semiconductor Integrated Circuits and Technology Symposium (BCICTS)*, 2018, pp. 231–234.

[20] R. Garg and A. S. Natarajan, "A 28-GHz Low-Power Phased-Array Receiver Front-End With 360° RTPS Phase Shift Range," *IEEE Trans. Microw. Theory Tech.*, vol. 65, no. 11, pp. 4703–4714, 2017.

[21] Z. Shen, A. Papasakellariou, J. Montojo, D. Gerstenberger, and F. Xu, "Overview of 3GPP LTE-Advanced Carrier Aggregation for 4G Wireless Communications," *IEEE Communications Magazine*, vol. 50, no. 2, pp. 122–130, 2012.

[22] 3GPP, "TS 38.104, Base Station (BS) Radio Transmission and Reception," 2019.

[23] P. Skrimponis, S. Dutta, M. Mezzavilla, , S. Rangan, S. H. Mirfarshbafan, C. Studer, J. Buckwalter, and M. Rodwell, "Power Consumption Analysis for Mobile MmWave and Sub-THz Receivers," in *Proc. IEEE 6G Wireless Summit*, 2020.

[24] P. Mogensen, W. Na, I. Z. Kovács, F. Frederiksen, A. Pokhariyal, K. I. Pedersen, T. Kolding, K. Hugl, and M. Kuusela, "LTE capacity compared to the Shannon bound," in *2007 IEEE 65th Vehicular Technology Conference-VTC2007-Spring*. IEEE, 2007, pp. 1234–1238.

[25] M. Giordani, M. Polese, A. Roy, D. Castor, and M. Zorzi, "A Tutorial on Beam Management for 3GPP NR at mmWave Frequencies," *IEEE Communications Surveys & Tutorials*, vol. 21, no. 1, pp. 173–196, 2018.